Polymer 327 (2025) 128403

Contents lists available at ScienceDirect

Polymer

journal homepage: www.elsevier.com/locate/polymer

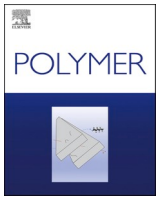

Rational design of glycidyl azide polymer-based triblock copolymers for high-performance energetic thermoplastic elastomers

Ming-Yen Tsai [a,1], Ming-Chieh Lin [a,1], Shih-Ya Hong [b], Yi-Chen Wu [a], Mohamed Gamal Mohamed [a], Shiao-Wei Kuo [a,c,*]

[a] Department of Materials and Optoelectronic Science, Center for Functional Polymers and Supramolecular Materials, National Sun Yat-Sen University, Kaohsiung, 804, Taiwan
[b] Chemical System Research Division, National Chung-Shan Institute of Science and Technology, Tao-Yuan, 325, Taiwan
[c] Department of Medicinal and Applied Chemistry, Kaohsiung Medical University, Kaohsiung, 807, Taiwan

ARTICLE INFO

Keywords:
Energetic thermoplastic elastomer
Glycidyl azide polymer
Triblock copolymer
Hydrogen bond

ABSTRACT

In aerospace applications, such as rockets and missiles, using thermoplastic elastomers (TPEs) in rocket propellants offers favorable properties that may allow them to replace traditional thermosetting elastomers. This study investigates the synthesis of energetic thermoplastic elastomers (ETPEs) with energetic characteristics, specifically focusing on synthesizing glycidyl azide polymer (GAP) ETPE and the effect of varying hard segment ratios on their physical properties. However, only the presence of azide side chains negatively impacts the mechanical properties of the ETPE and to address this issue, an ABA triblock copolymer synthesis approach is employed, utilizing poly (ε-caprolactone) (PCL) long linear chains to modify the original GAP, forming PCL-GAP-PCL ETPE. The introduction of PCL-GAP-PCL triblock copolymers significantly enhanced the mechanical properties of the resulting ETPE, providing substantial benefits for its use in specific environments. Furthermore, this study also investigates the effects of varying soft/hard segment ratios in the ETPE, suggesting that the subsequent incorporation of oxidizer fillers could yield favorable mechanical properties. Additionally, 2D infrared spectroscopy (2D-IR) was utilized to understand the effects of hydrogen bond formation and dissociation.

1. Introduction

Energetic materials are frequently applied in the aerospace and defense industries [1–4]. In the aerospace field, the focus is primarily on satellite systems and the rapidly growing rocket launch industry. Propulsion systems, which are the core of rocket power, could be categorized into solid, liquid, and hybrid propellants [5–7]. Liquid propellants often face storage challenges, particularly with oxidizers, complicating storage conditions and imposing higher demands on the materials of rocket components, thereby significantly increasing costs. Consequently, there has been growing interest in improving solid propellants. Traditionally, thermosetting propellants have been used, but they also present several challenges, and solid rocket propellants are typically processed using either thermosetting or thermoplastic methods. Traditional thermosetting propellants, such as hydroxyl-terminated polybutadiene (HTPB) propellants, offer advantages such as high solid content, high density, high specific impulse (I_{sp}), good safety, and low cost [8]. However, their manufacturing process is complex, involving multiple steps such as pre-mixing, mixing, casting, curing, demolding, and shaping. These processes require specialized molds to control the grain shape, making it difficult to produce complex grain geometries. Furthermore, the process and storage are susceptible to moisture. These issues have led to increasing interest in developing thermoplastic elastomers for use in propellants, which has become an important area of research [9,10].

Compared to traditional thermosetting propellants, thermoplastic propellants offer several advantages, including ease of processing, no pot-life limitations, fast curing, low sensitivity to moisture, low toxicity (or even non-toxicity), and reprocessability. These characteristics suggest that thermoplastic propellants have the potential to serve as green propellants [11]. In the application of thermoplastic propellants, the use of energetic thermoplastic elastomers (ETPEs) as binders offers notable

* Corresponding author. Department of Materials and Optoelectronic Science, Center for Functional Polymers and Supramolecular Materials, National Sun Yat-Sen University, Kaohsiung, 804, Taiwan.
E-mail address: kuosw@faculty.nsysu.edu.tw (S.-W. Kuo).
[1] These authors contributed equally to this work.

https://doi.org/10.1016/j.polymer.2025.128403
Received 31 December 2024; Received in revised form 17 March 2025; Accepted 12 April 2025
Available online 14 April 2025

superiority. Polymers like poly (3-nitratomethyl-3-ethyloxetane) (Poly (NiMMO)) [12], glycidyl azide polymer (GAP) [13,14], Poly (GlyN) [15], poly (3,3-bis(3-azidomethyl)oxetane) (PBAMO) [16], and poly (3-azidomethyl-3-methyloxetane) (PAMMO) [17], are favored due to their energetic properties, stemming from their azido and nitro functional groups. Among these polymers, GAP has garnered particular attention for its excellent properties as an ETPE binder. Despite the relatively rigid backbone and side-chain structure of GAP [18], its relatively straightforward two-step synthesis and cost-effectiveness make it an excellent candidate for developing ETPEs. GAP could enhance compatibility with oxidizers and increase the energy density of propellant formulations [19–22]. Even though GAP has been widely investigated as a propellant binder, its inherent mechanical performance is limited, making it insufficient for certain applications [23–25].

In this study, we aimed to enhance the mechanical properties, flexibility, and thermoplasticity of GAP-ETPE. Polycaprolactone (PCL) is a semicrystalline, biodegradable polymer from the aliphatic polyester family, known for its excellent mechanical properties, making it suitable for thermoplastic processing [26–29]. To achieve this, we introduced the concept of a triblock copolymer by modifying GAP with ester-based segments to improve its flexibility during elastomer formation. Specifically, PCL was tethered onto both ends of GAP to serve as a flexible segment. PCL, a common soft segment in polyurethane (PU) synthesis, consists of flexible molecular chains with five nonpolar methylene (–CH_2–) groups and one polar ester (–COO–) group. Polytetramethylene ether glycol (PTMEG) has four methylene (–CH_2–) groups and one ether oxygen (–O–), offering low polarity and excellent flexibility due to its low glass transition temperature (T_g). While PCL has a slightly higher T_g, its semicrystalline nature ensures good elasticity. In contrast, polyethylene oxide (PEO), composed of ethylene glycol (–CH_2–CH_2–O–) units, exhibits higher crystallinity and chain rigidity, limiting its flexibility [30,31]. Therefore, PCL is a suitable modifier for GAP due to its flexibility, cost-effectiveness, and ability to enhance the toughness of the soft segment without requiring additional plasticizers [32,33]. We compared the performance of ETPEs synthesized using pure GAP homopolymer as a polyol with those using PCL-GAP-PCL triblock copolymers, which were synthesized with 4,4′-methylene bis(cyclohexyl isocyanate) (HMDI) and 1,4-butanediol (1,4-BDO) as the hard segment. The molecular weight of the PCL-GAP-PCL triblock copolymer was designed to be comparable to that of the GAP homopolymer, and under similar conditions, we successfully fabricated energetic thermoplastic elastomers. Notably, the synthesized PCL-GAP-PCL ETPE not only retained its energetic properties but also exhibited excellent thermoplasticity and significantly improved mechanical performance. We also investigate the effect of the hard segment ratios on the properties of GAP-based energetic thermoplastic elastomers (GAP-ETPE) and explore the impact of incorporating triblock copolymer of PCL-GAP-PCL ETPE on enhancing the mechanical properties of the elastomers. Additionally, the influence of hydrogen bonding interaction in polyurethane on the thermoplastic performance is also examined.

2. Experimental section

2.1. Materials

(±)-Epichlorohydrin (ECH, 99 %), 2,2-bis(bromomethyl)-1,3-propanediol, boron trifluoride diethyl etherate (BTFE, 98 %), the isocyanate and the chain extender used in the synthesis of ETPE were 4,4′-methylenebis (cyclohexyl isocyanate) (HMDI, 90 %) were obtained from Thermo Scientific. Analytical grade chemicals, including dichloromethane (DCM), *n*-hexane, tetrahydrofuran (THF), ethyl acetate (EA), and N,N-dimethylformamide (DMF) were sourced from Acros Organics. Sodium azide (NaN_3), sodium chloride (NaCl), and magnesium sulfate anhydrous ($MgSO_4$) were procured from SHOWA. The ε-caprolactone monomer (ε-CL) was sourced from Sigma-Aldrich and dehydrated using CaH_2 for one day. Dibutyltin dilaurate (DBTDL, 95 %) was obtained from Tokyo Chemical Industry (TCI). 1,4-Butanediol (1,4-BDO, 99 %) was purchased from Alfa Aesar.

2.2. Synthesis of polyepichlorohydrin (PECH) [34]

2,2-Bis(bromomethyl)-1,3-propanediol and boron trifluoride diethyl etherate acted as initiator and catalyst, respectively, and were placed in a 500 mL three-neck round bottom flask. After that, DCM was added to dissolve the solid, and then the flask was treated under a nitrogen atmosphere. The mixture was stirred with a magnetic stirrer at ambient temperature for 30 min and then cooled in an ice bath. Subsequently, the ECH monomer was added dropwise at approximately 65 mL/h. The mixture reacted for 4 h and then terminated. Finally, the solution was purified by extracting it three times with 200 mL of saturated NaCl aqueous solution. The organic layer was dried over anhydrous $MgSO_4$, and filtered, and the DCM was removed by rotary evaporation to obtain $PECH_{19}$ with a yield of approximately 96 wt% and $PECH_8$ with a yield of approximately 83 wt%.

2.3. Synthesis of glycidyl azide polymer (GAP) [34]

PECH obtained was placed into a three-neck flask with an excess of NaN_3 and 200 mL of DMF. The mixture was heated to 120 °C and reacted for 24 h. After cooling, unreacted NaN_3 and by-products NaCl were removed by filtration. The product was then concentrated by rotary evaporation to remove the DMF solvent, yielding the crude product GAP homopolymer. The crude product was dissolved again in EA and extracted three times with saturated NaCl aqueous solution. The organic layer was concentrated by rotary evaporation to obtain GAP homopolymer.

2.4. Synthesis of PCL-GAP-PCL triblock copolymer

To better investigate the differences between pure GAP homopolymer and PCL-GAP-PCL triblock copolymer when used as polyols, we synthesized them with as similar molecular weights as possible for comparison. PCL-GAP-PCL triblock copolymer with different molecular weights was synthesized through ring-opening polymerization by using GAP_8. The reactions were carried out with GAP_8 and ε-CL at weight ratios of 1:1, 1:2, and 1:4. Approximately DBTDL (0.3 mL) was used as a catalyst, and the mixture was degassed by freeze drying to remove water. The reaction was performed under a nitrogen atmosphere by heating to 120 °C for 24 h. Three types of PCL-GAP-PCL triblock copolymers were obtained for comparison.

2.5. Synthesis of the HMDI-Based GAP-ETPE and PCL-GAP-PCL ETPE

GAP and PCL-GAP-PCL triblock copolymers, which serve as polyols, as soft segments. These were pretreated by placing them in an oven at 90 °C for 2 h. After removal, they were reacted into a three-neck flask. The flask was equipped with a mechanical stirrer, and the system was subjected to vacuum and nitrogen purging three times to maintain an inert nitrogen atmosphere. Subsequently, catalyst DBTDL (0.25 mL) was added to the flask and stirred thoroughly. The temperature was then raised to 90 °C. HMDI, representing the hard segment, was withdrawn using a syringe to prevent direct exposure to ambient moisture. It was swiftly injected into the flask, and the reaction proceeded for 2 h. Afterward, 1,4-BDO was placed in an 80 °C oven for 1 h as the hard segment and chain extender. Following the completion of the prepolymer reaction, the temperature was lowered to 60 °C. 1,4-BDO was added and stirred continuously until homogeneous. The entire reaction mixture was then transferred into a suitable container and placed in an oven for a curing reaction at 100 °C for 24 h. The hard segment (HS) weight fraction of ETPE was calculated by using $HS\% = (W_{HMDI} + W_{1,4-BDO})/(W_{HMDI} + W_{1,4-BDO} + W_{polyol})$. The mass of the energetic polyol, HMDI, and 1,4-BDO used in the calculation are provided in

Tables S2 and S3.

3. Results and discussion

In this study, Fig. 1(a) illustrates that PECH uses 2,2-bis(bromomethyl)-1,3-propanediol with two Br atoms as an initiator to obtain more substituted azido group positions. ECH undergoes cationic ring-opening polymerization through the activated monomer (AM) mechanism to form a linear structure, avoiding the activated chain end (ACE) mechanism that leads to cyclization structures [35]. The molecular weight is controlled by the concentration ratio. Table S1 summarizes the synthesis conditions of $PECH_8$ and $PECH_{19}$. As displayed in Fig. 1(b), FTIR spectra confirm the presence of characteristic absorption peaks for PECH in the fingerprint region, specifically C–Cl at 748 cm^{-1} and C–Br at 701 cm^{-1}. These sites are replaced by azido groups during the azidation reaction, leading to the disappearance of these signals. A strong and narrow peak at 2102 cm^{-1} indicates the presence of azido groups, while the C–N bond is observed at 1284 cm^{-1}. Thus, the successful azidation of PECH to GAP is confirmed by FTIR analysis. Through analysis of the ^{1}H NMR and ^{13}C NMR spectra, proton signals corresponding to ether units and those attached to Cl and azido groups can be observed between 3.4 and 3.7 ppm. The peak observed at 3.5 ppm corresponds to the proton signal of C**H**$_2$–Br, while the peak at 3.6 ppm represents the proton signal of C**H**$_2$–Cl in the repeating unit of ECH. After the azide reaction forms GAP, the halogen sites are replaced by N_3, causing the proton signal to shift to 3.33 ppm (-C**H**$_2$-N_3) (Fig. 1(c)). In the ^{13}C NMR spectra, the signals for ether groups are more clearly distinguished. The chemical shift positions for the carbon atoms in **C**H_2–Cl and **C**H_2–Br at 44.1 ppm and 34.5 ppm respectively shifted to 51.5 ppm and 53.1 ppm after being substituted by the azido group as **C**H_2–N_3. The **C**H carbon signal in O–CH_2–**C**H appears at 79.1 ppm, and the **C**H_2 signal is at 70.4 ppm. The presence of multiple **C**H_2 signals suggests that grafting may occur in head-to-head, head-to-tail, and tail-to-tail configurations simultaneously (Fig. 1(d)) [36]. Additionally, we analyzed the molecular weight of the synthesis $PECH_{19}$ and GAP_{19} based on the integral of the signals obtained from the ^{1}H NMR spectrum, as summarized in Table S2. The azidation phenomenon can also be observed from GPC analysis. The synthesized samples show a relatively narrow PDI value of approximately 1.10.

A slight shift in the GPC curve indicates an increase in molecular weight (Fig. S1). Additionally, we used MALDI-TOF mass spectrometry to obtain mass spectrometry signals. Each signal unit was quite consistent, with *m/z* of 1098.67 and 999.17, showing a difference of approximately 99 Da, corresponding to the molecular weight of GAP. The signals between them, differing by about 14 and 28 Da, correspond to the splitting of the azido group into N and N_2. By observing approximately 19 signals and applying the formula, the molecular weight was determined to be approximately 2057 Da (Fig. 1(e)). Fig. 1(f) shows that due to the azidation reaction, the T_g of PECH decreased from −43 °C to the T_g of GAP at −61 °C. This occurs because the original strongly polar Cl atom is replaced by linear azido groups, which change the molecular mobility characteristics and increase flexibility, resulting in a lower T_g [37]. From the TGA analysis of thermal decomposition, it can be observed that GAP_{19} reaches T_{d5} at 231 °C, while $PECH_{20}$ reaches this point at 287 °C. The data shows that PECH undergoes significant thermal decomposition between 300 °C and 350 °C, whereas GAP exhibits the first stage of weight loss between 250 °C and 282 °C. This weight loss may be attributed to the decomposition of azido groups, leading to the

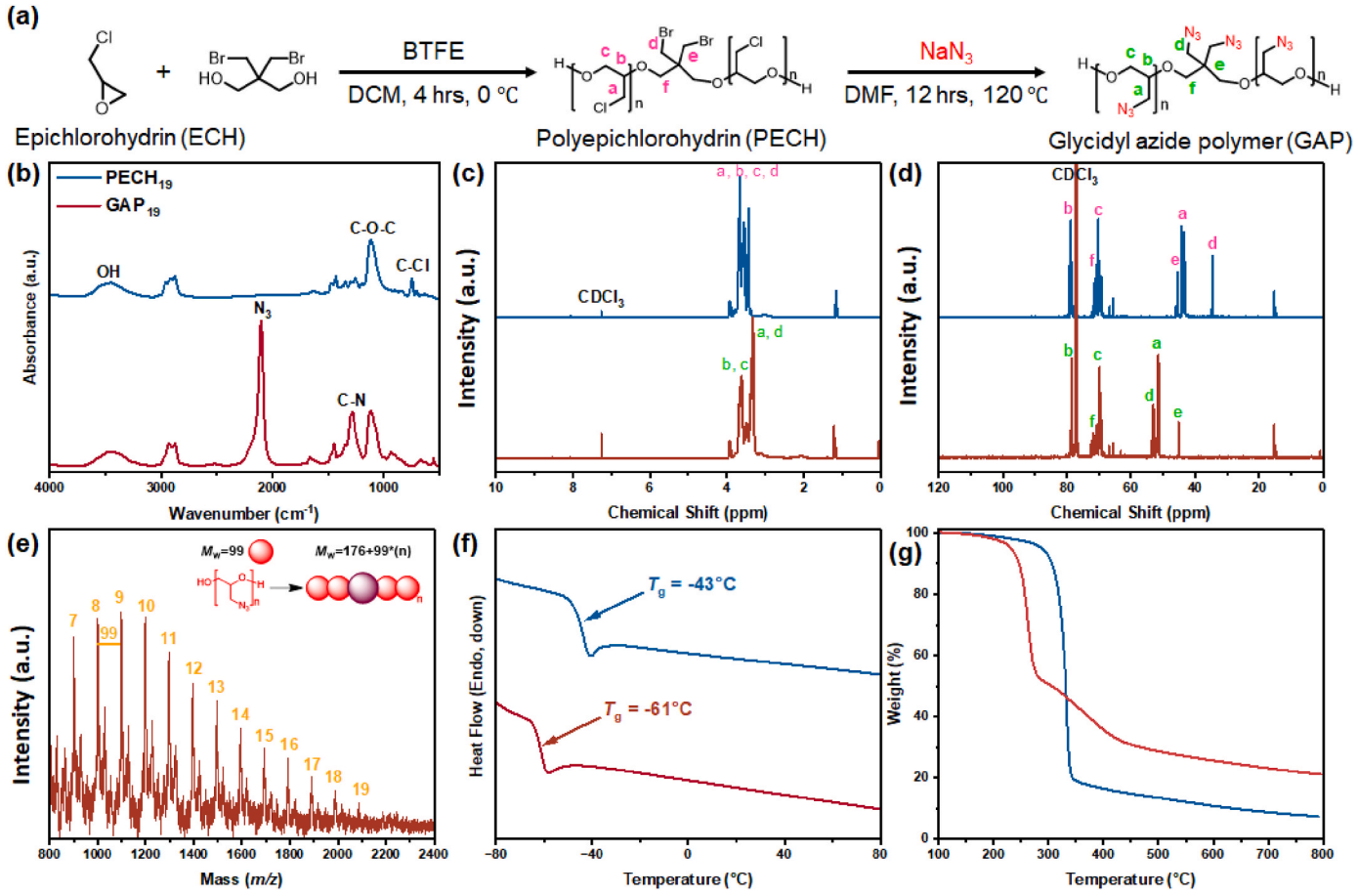

Fig. 1. Schematic diagram and structural characterization of GAP_{19}. (a) Chemical structures of $PECH_{19}$ and GAP_{19}. (b) FTIR spectra. (c) ^{1}H NMR spectra. (d) ^{13}C NMR spectra of $PECH_{19}$ and GAP_{19}. (e) MALDI-TOF MS spectrum of GAP_{19}. (f) DSC thermogram. (g) TGA analyses of $PECH_{19}$ and GAP_{19}.

release of N_2. Part of the C–N bonds cyclize at higher temperatures, forming a cross-linked network structure [38], while the remaining ether groups continue to decompose from 282 °C to 435 °C. As a result, GAP demonstrates a higher char yield compared to PECH, approximately 21.1 wt% (Fig. 1(g)) [39].

This study introduces ester-containing triblock energetic GAP for investigation. Before synthesizing ETPE, we explored the PCL-GAP-PCL triblock copolymer and compared it to pure GAP homopolymer as a polyol as shown in Fig. 2(a). To control for similar molecular weights, the experiment was designed with a triblock ratio of 0.5:1:0.5 for PCL-GAP-PCL, targeting approximately 2000 g/mol. Therefore, a low molecular weight glycidyl azide polymer of about 1000 g/mol was first synthesized as an intermediate. By increasing the ratio of catalyst to initiator, GAP_8 with a molecular weight of about 1000 g/mol was successfully synthesized. GAP_8 was then grafted with CL through ring-opening polymerization to form a PCL-GAP-PCL triblock copolymer with different weight ratios. Fig. 2(b) shows that the FTIR spectra of GAP_8 have the same azido functional group at 2100 cm^{-1} as GAP_{19}. In the analysis of PCL-GAP-PCL triblock copolymer, the successful graft of PCL is confirmed by the presence of the same azide signals in the energetic structure. The 1724 cm^{-1} and 1734 cm^{-1} regions show the C=O crystalline and amorphous signals of the PCL segment, respectively, and as the amount of grafted PCL increases, the ratio of these two signals indicates a weakening of the azide signal. Fig. 2(c) and (d) show the ^1H and ^{13}C NMR spectra of the copolymer. As previously mentioned, the GAP signals are observed between 3.4 and 3.7 ppm. At 2.24 ppm, protons adjacent to the C**H**$_2$–C (=O) carbonyl group of PCL are detected. The signals at 1.27, 1.55, and 1.58 ppm correspond to the methylene protons of PCL after ring-opening polymerization. In the ^{13}C NMR spectrum, the methylene carbon signals of PCL are observed at 24.3, 25.2, 28.1, and 33.8 ppm. The carbon signal for the O-(**C**H$_2$) group is found at 63.9 ppm, and the carbon signal for the PCL carbonyl group -**C**(=O)- is at 173.4 ppm. To further confirm that the synthesized PCL-GAP-PCL triblock copolymer is composed of uniform chain segments, we employed NMR diffusion-ordered spectroscopy (DOSY) for analysis. As shown in the upper projection of the ^1H NMR signals in Fig. 2(e), the DOSY spectrum for PCL_5-GAP_8-PCL_5 exhibits the same diffusion coefficient across the sample. This consistency indicates that the ring-opening polymerization was successfully conducted and suggests that there are no residual small molecules present in the final product, confirming the uniformity of the synthesized copolymer [40,41]. Fig. 2(f) shows the DSC thermal analysis of low molecular weight GAP_8. Although it has a lower molecular weight compared to GAP_{19}, there is no significant difference in their T_g values, which are relatively close. GAP_8 has a glass transition temperature (T_g) of −59 °C, while pure PCL has a T_g of approximately −70 °C. The incorporation of GAP into the triblock structure results in an overall decrease in T_g. It is observed that as the amount of tethered PCL increases, the T_g shows a slight and continuous decrease. Additionally, during the cooling process, the triblock materials exhibit cold crystallization (Fig. S6). Since GAP is amorphous and PCL segments can crystallize, as noted in previous studies, the crystallization peaks observed during cooling can be attributed to the PCL blocks [42].

The presence of crystallization and two melting peaks is due to the PCL segments and is also influenced by the intermediate GAP segments [43,44]. From the TGA in Fig. 2(g), it is observed that the majority of thermal degradation for GAP_8 occurs between 150 °C and 280 °C,

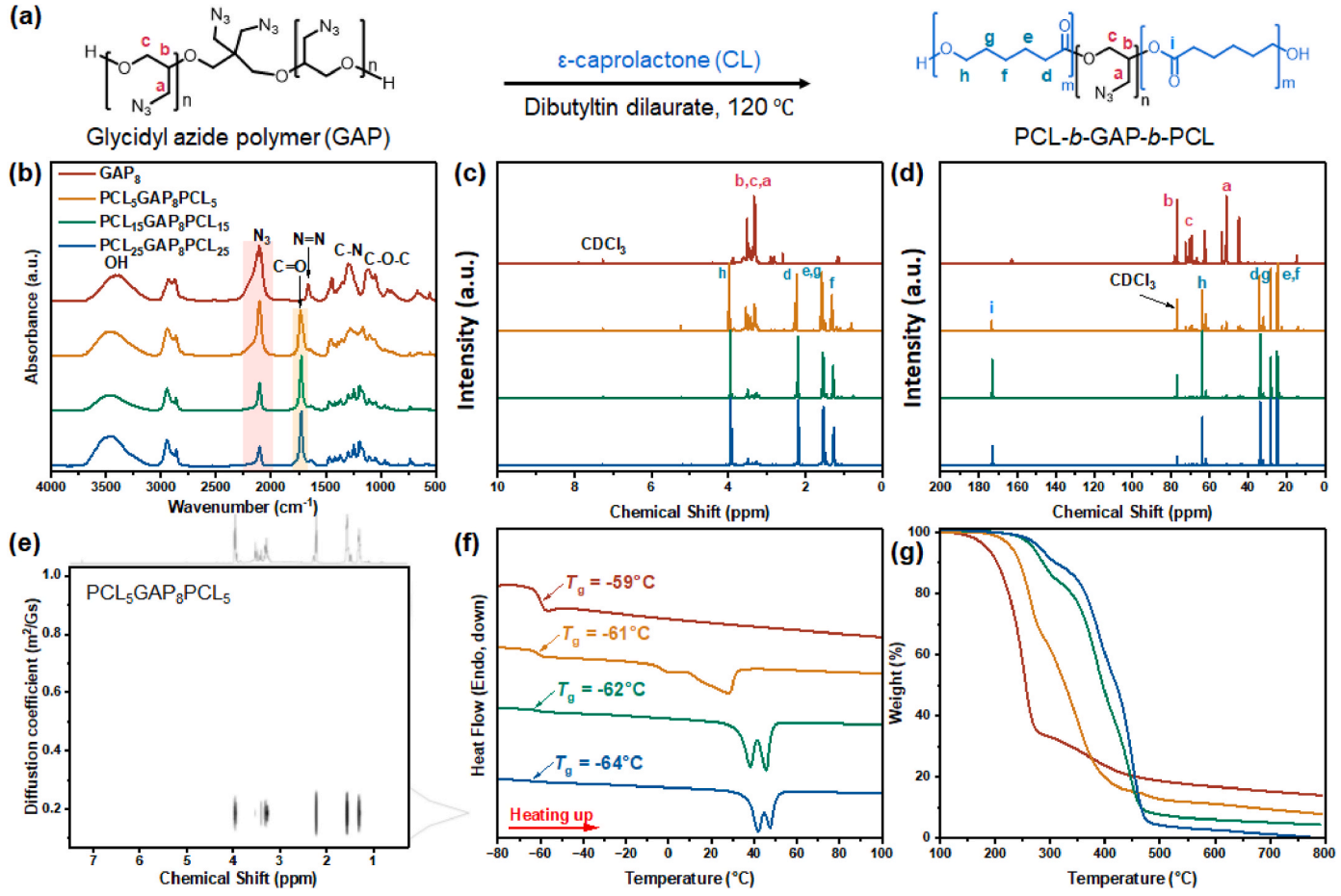

Fig. 2. Schematic and structural characterization of PCL-*b*-GAP-*b*-PCL triblock copolymer. (a) Chemical structure of the PCL-*b*-GAP-*b*-PCL triblock copolymer. (b) FTIR spectra. (c) ^1H NMR spectra. (d) ^{13}C NMR spectra of PCL-*b*-GAP-*b*-PCL triblock copolymer. (e) DOSY spectrum of $PCL_5GAP_8PCL_5$. (f) DSC thermogram of PCL-*b*-GAP-*b*-PCL. Inset: cooling scan. (g) TGA analyses of PCL-*b*-GAP-*b*-PCL triblock copolymer.

resulting in an overall weight loss of 65 wt%. It is speculated that while some segments undergo degradation, partial crosslinking occurs, leaving a char yield of 14 wt%. Furthermore, for these three samples containing PCL blocks, it is observed that as the number of PCL blocks increases, the degradation temperature of GAP also increases. After the degradation of GAP, the PCL segments undergo degradation as well. As the proportion of PCL blocks increases, the degree of crosslinking decreases, leading to a reduction in char yield. Overall, PCL successfully undergoes ring-opening polymerization and is tethered to GAP homopolymer. As the proportion of PCL increases, the amount of PCL tethered also increases, leading to a decrease in the original GAP signals and an increase in PCL signals, which influences the thermal properties of the original GAP. To analyze molecular weight variations, we utilized GPC, MALDI-TOF mass spectrometry, and ^{1}H NMR signal integration for cross-validation. The GPC spectra indicate that as the amount of PCL increases, the peak shifts toward higher molecular weights (Fig. S4). Additionally, the MALDI-TOF mass spectrometry analysis shown in Fig. 3 supports the GPC data by demonstrating that higher molecular weights increase fragment ions. Moreover, the analysis of two mass peaks for PCL-GAP-PCL triblock copolymers consistently shows an increase of 114 Da, corresponding to the PCL segment, indicating successful grafting of PCL onto the polymer main chain. The primary method used for determining the ratio of the PCL chain in the synthesis and estimating the molecular weight was through the integration of ^{1}H NMR signals. The results are summarized in Table S3.

We used the GAP_{19} and $PCL_5GAP_8PCL_5$ as polyols to react with isocyanate (HMDI) and chain extender (1,4-BDO) to synthesize energetic thermoplastic elastomers (ETPEs) [Fig. 4(a) and Table S4]. From the FTIR analysis in Fig. 4(b) and **5(b)**, the azido functional group can be observed at 2109 cm^{-1}, indicating that the energetic azide functionality is retained after synthesizing ETPE. After attaching HMDI and the chain extender (1,4-BDO), the original OH stretch at 3429 cm^{-1} disappears, and the NH stretch of the hard segment HMDI appears at 3316 cm^{-1}. Additionally, the signal at 1522 cm^{-1} can be attributed to C (=O)–**NH**. At 1707 cm^{-1}, the C=O signal is observed in the pure GAP-ETPE series. In comparison, the PCL-GAP-PCL-ETPE series shows a C=O signal that partially originates from the PCL segments and partially from the C=O in HMDI, both providing sites for hydrogen bonding. The –NCO signal at 2271 cm^{-1}, present in the HMDI raw material, disappears after the reaction (Fig. S4), indicating the successful formation of ETPE. Furthermore, the NH wagging at 779 cm^{-1} increases with the proportion of the hard segment, as indicated by the rise in absorbance. Fig. 4(d) and **(e)** show the NMR spectra of the GAP-ETPE series, with individual analyses of the ^{1}H and ^{13}C NMR spectra. In the ^{1}H NMR spectrum, the C**H**$_2$ signal linking the two cyclohexane rings of HMDI is found at 0.94 ppm. The alicyclic signals of the cyclohexane ring are observed at 1.10 ppm, 1.96 ppm, and 3.4 ppm. The proton signal of C (=O)–N**H** appears at 4.94 ppm. Two C**H**$_2$ signals from the chain extender 1,4-BDO are observed at 1.56 ppm and 1.67 ppm, and the O–C**H**$_2$ signal is at 3.76 ppm. The terminal O**H** proton signal is observed at 4.06 ppm. These signals are present at the same positions for different hard segment ratios. In the ^{13}C NMR spectra, the HMDI carbon signals are found at 28.1 ppm, 29.5 ppm, 32.1 ppm, and 45.1 ppm. Peaks at 154.7 ppm and 156 ppm indicate the successful attachment of HMDI to the polyol and chain extender, respectively, showing two different chemical environments for **C**=O units. Carbon signals of 1,4-BDO are observed at 25 ppm, 63.1 ppm, and 64.8 ppm. These results confirm the successful synthesis of GAP-ETPE. Fig. 5(d) and **5(e)** show the NMR spectra of PCL-GAP-PCL ETPE. The spectra also exhibit the proton and carbon signals of HMDI and 1,4-BDO, along with the inherent peaks of the triblock copolymer, confirming the successful synthesis of PCL-GAP-PCL ETPE. The molecular weights of the synthesized ETPEs were confirmed using GPC, as detailed in Table S5. In Fig. 4(c), the thermal properties of GAP-ETPE are displayed. After forming the elastomer, an increase in the T_g is observed, which further rises with a higher proportion of the hard segment.

The T_g obtained serves as a reference for practical applications in various environments. The inset in the top corner shows that when heating continues to 300 °C, thermal decomposition of ETPE begins around 200 °C and peaks at approximately 250 °C. Comparing this with the combustion heat peak of pure GAP_{19} at 2386 J/g, the elastomer shows a reduction in combustion heat as the hard segment ratio increases. For GAP-ETPE with 40 %, 45 %, and 50 % hard segments, the combustion heat peaks at around 1390 J/g, 1338 J/g, and 1282 J/g, respectively. This confirms that the elastomer retains its energetic

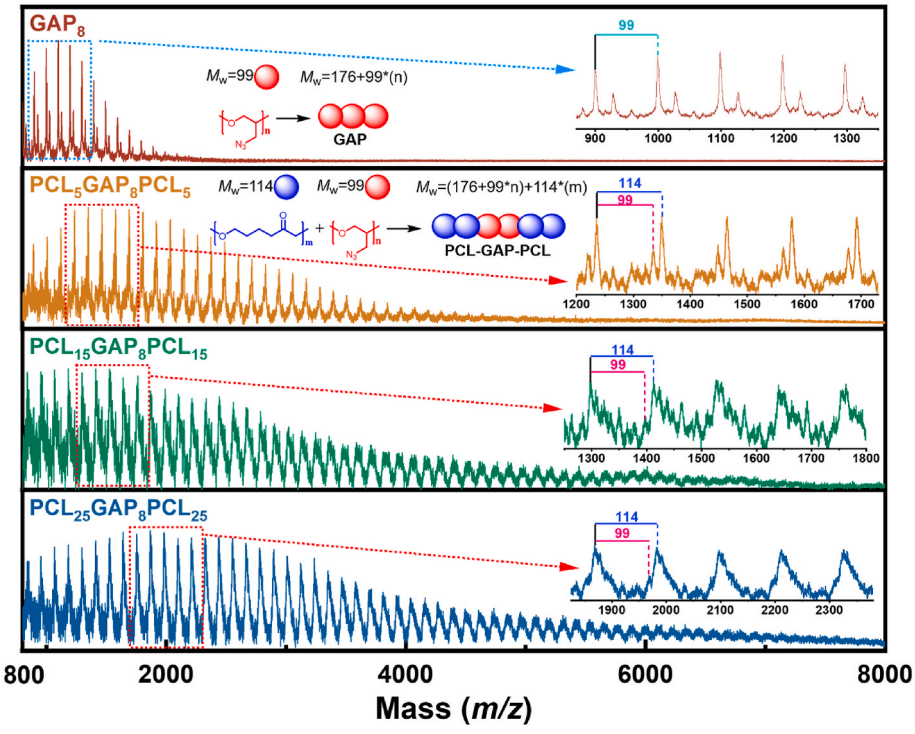

Fig. 3. MALDI-TOF MS spectra of PCL-GAP-PCL triblock copolymers with varying PCL compositions.

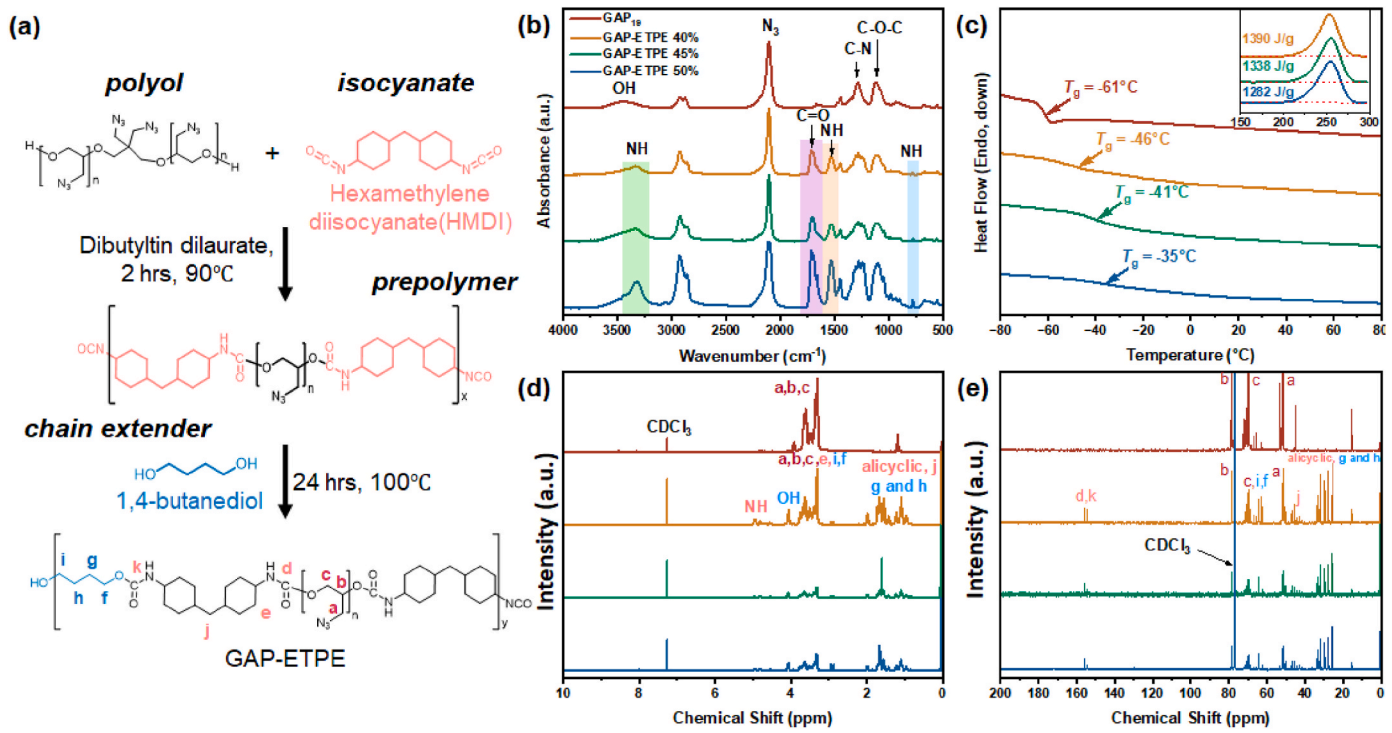

Fig. 4. Schematic and structural characterization of GAP-ETPE. (a) Chemical structure of GAP-ETPE. (b) FTIR spectra of the three hard segments in GAP-ETPE. (c) DSC thermograms of the three hard segments in GAP-ETPE. Inset: DSC thermograms of the heat release. (d) ^{1}H NMR spectra of the three hard segments in GAP-ETPE. (e) ^{13}C NMR spectra of the three hard segments in GAP-ETPE.

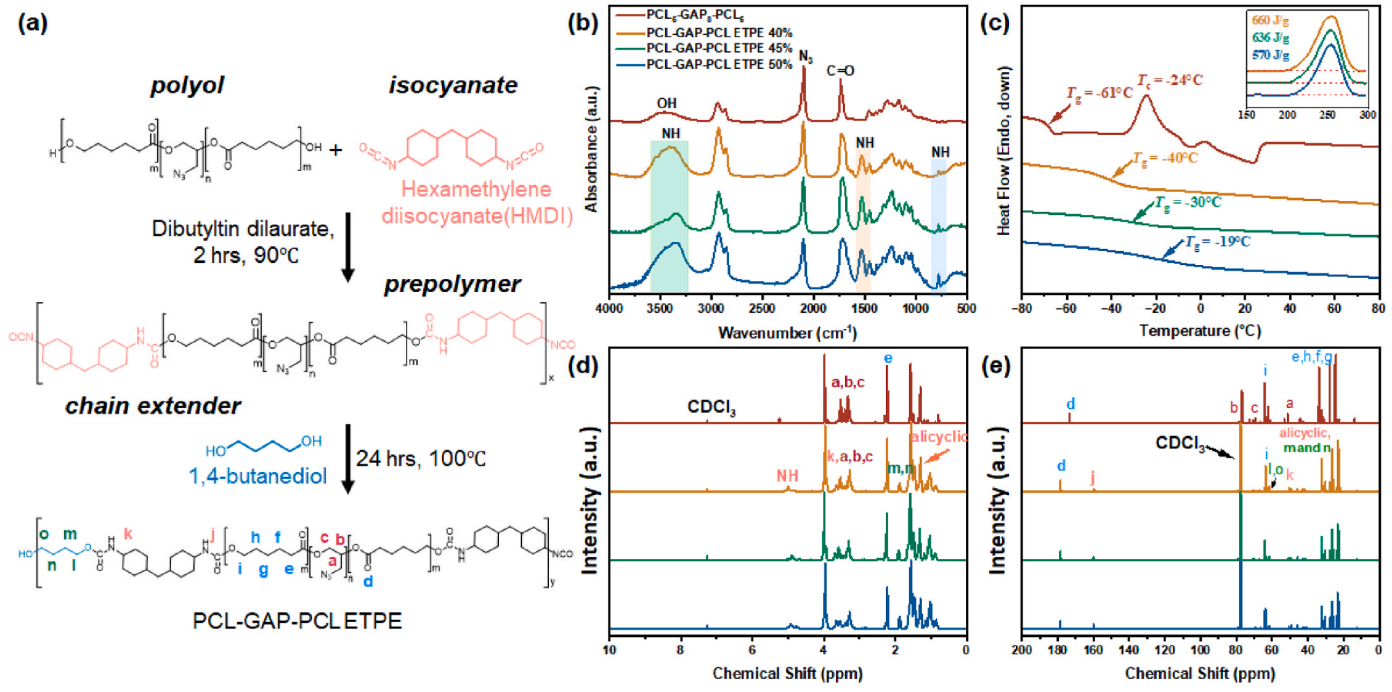

Fig. 5. Schematic and structural characterization of PCL-GAP-PCL ETPE. (a) Chemical structure of PCL-GAP-PCL ETPE. (b) FTIR spectra of the three hard segments in PCL-GAP-PCL ETPE. (c) DSC thermograms of the three hard segments in PCL-GAP-PCL ETPE. Inset: DSC thermograms of the heat release. (d) ^{1}H NMR spectra of the three hard segments in PCL-GAP-PCL ETPE. (e) ^{13}C NMR spectra of the three hard segments in PCL-GAP-PCL ETPE.

properties after fabrication. In Fig. 5(c), the thermal properties of PCL-GAP-PCL ETPE are presented. Due to the presence of PCL segments, crystallization occurs, and after ETPE formation, some PCL segments may remain within the structure. This restricts molecular motion, causing the T_g of PCL-GAP-PCL ETPE to be higher than that of GAP-ETPE. However, overall, crystallization does not occur within the elastomer. The inset also shows a combustion heat peak after 200 °C. Since the polyol used contains only 8 GAP repeat units, the combustion heat peak for PCL-GAP-PCL ETPE is 1152 J/g, which is relatively lower—about 50 % of the energetic capacity—compared to pure GAP-ETPE. The

DSC diagrams and data of GAP_{19} and PCL_5-GAP_8-PCL_5 are shown in Fig. S5.

The elastomers we designed retain thermoplastic properties and can be cast above softening temperature and hardened at room temperature. Each sample underwent a complete 24 h curing process at 100 °C. Fig. 6 (b) demonstrates the flow behavior of pure GAP-ETPE with 40 % hard segment when heated above its softening temperature, while it maintains a solid, molded state when stored at room temperature. In this study, five out of the six materials exhibited solidifying behavior at room temperature. In particular, pure GAP-ETPE at 40 %, 45 %, and 50 %, as well as PCL-GAP-PCL ETPE at 45 % and 50 % hard segment. Only PCL-GAP-PCL ETPE at 40 % hard segment failed to form a solid shape at room temperature. Fig. 6(a) illustrates the role of hydrogen bonding within the system. At room temperature, specific functional groups within the ETPE molecules can form hydrogen bonds, which tighten the molecular structure, allowing the material to solidify [45]. However, as the temperature increases, these hydrogen bonds are gradually disrupted until they dissociate, causing the material to exhibit flow behavior. This can be attributed to the polyol design, which is diol-based and prevents the molecule from forming a crosslinked network after thermal curing. Additionally, the thermal properties of the hydrogen bonds play a critical role. Fig. 6(c) shows that the solidifying ETPE exhibits a first-order phase transition during the first scan in DSC. Due to insufficient time to form hydrogen bonds during the second cooling and heating cycle, no endothermic behavior is observed in this scan. The endothermic peak observed during the first scan corresponds to the softening temperature of the elastomer. Samples that cannot be molded do not show any phase transition peaks in either the first or second scan [46]. In Fig. 6(d), we observe the rheological properties of ETPE under temperature variation. The data indicates that as the proportion of hard segments increases, the initial viscosity of the ETPE rises. However, as the temperature increases and hydrogen bonds break, molecular mobility increases, leading to a decrease in viscosity. During temperature ramp scans, the relationship between G′ (storage modulus) and G″(loss modulus) is used to determine the material's state. When $G' > G''$, the material is in a solid state, while $G'' > G'$ indicates a liquid state and higher then softening temperature. The phase transition temperature, where $G' = G''$, defines the softening point.

For instance, the softening point of pure GAP-ETPE with 40 % hard segment is 107 °C, and PCL-GAP-PCL ETPE with 50 % hard segment has a softening point of 123 °C. The temperature-dependent rheological data for all prepared ETPEs are shown in Fig. S7. The data reveals that the ETPEs that could be cast exhibit a distinct softening point, except for PCL-GAP-PCL ETPE with 40 % hard segment, which could not be solidified. During the scanning process, $G'' > G'$ was observed for these materials. These observations from DSC and rheological measurements correlate well, reflecting the microscopic phase changes and macroscopic behavior, respectively. Therefore, we further explored hydrogen bonding by introducing external perturbations and analyzed GAP-ETPE 50 % and PCL-GAP-PCL ETPE 50 % separately. Using FTIR, we measured the changes in signals between 60 °C and 180 °C. As shown in Fig. 6(e), the upper part of the figure presents GAP-ETPE 50 %. The left side corresponds to the N–H signal, while the right side corresponds to the C═O signal. With increasing temperature, the C═O peak at 1661 cm^{-1}, which was initially involved in hydrogen bonding interactions, gradually dissociates. Simultaneously, the signal at 1713 cm^{-1} progressively shifts to higher wavenumbers, indicating free C═O. Similarly, the N–H signal, which was originally observed at 3334 cm^{-1} under hydrogen

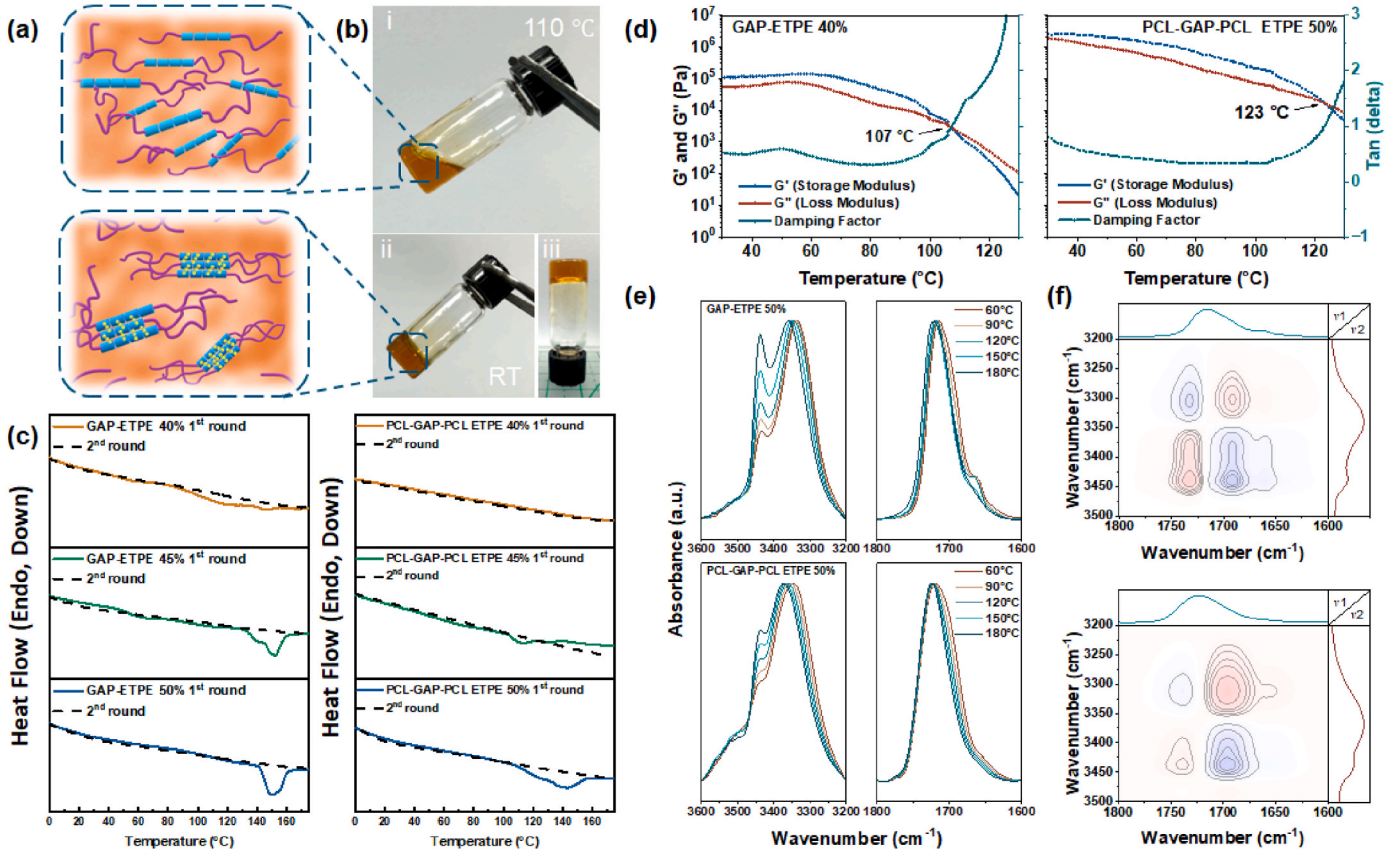

Fig. 6. Thermal property and hydrogen bonding analyses of ETPE elastomers. (a) The effect of hydrogen bonding on the internal separation of ETPE at different temperatures. (b) i. Photographs of GAP-ETPE 40 % at 110 °C; ii. and iii. Photographs of GAP-ETPE 40 % at room temperature. (c) DSC spectra of ETPE showing two scanning cycles. (d) Temperature-dependent rheological scans of GAP-ETPE 40 % and PCL-GAP-PCL ETPE 50 %. (e) Temperature-dependent IR spectra of GAP-ETPE 50 % and PCL-GAP-PCL ETPE 50 %. (f) 2D-IR spectra of GAP-ETPE 50 % and PCL-GAP-PCL ETPE 50 %.

bonding influence, shifts to higher wavenumbers as the hydrogen bonds are disrupted Additionally, with the increase in free N–H, the signal at 3438 cm^{-1} becomes stronger. This behavior is also observed in PCL-GAP-PCL ETPE 50 %. Notably, because PCL contains C═O, it also provides hydrogen bonding sites along with C═O in HMDI. As shown in the figure, the C═O peak at 1617 cm^{-1} is broader at 60 °C, indicating it is also influenced by hydrogen bonding. However, as the temperature increases and hydrogen bonds are disrupted, the peak becomes narrower and shifts. This analysis was further advanced by performing 2D FTIR to interpret the spectra, as shown in Fig. 6(f) [47–50]. The plot more clearly reveals the correlation between signals in the blue region, indicating a relationship between them. When hydrogen-bonded C═O forms, the amount of free N–H correspondingly decreases. As hydrogen-bonded N–H increases, the amount of free C═O decreases. The 2D FTIR analysis provides this critical information. This data further clarifies the essential role that hydrogen bonding plays in the ETPE.

Fig. 7(a) illustrates the processing of the PCL-GAP-PCL ETPE with 50 % hard segment sample, which was heated above its softening temperature and then directly cast into a silicone mold (Fig. 7(a–i)). After cooling to room temperature, the material was removed from the mold to form a dumbbell-shaped specimen (Fig. 7(a-ii)), demonstrating good elongation capability (Fig. 7(a-iii)). Except for the PCL-GAP-PCL ETPE with 40 % hard segment sample, which could not be solidified, the remaining five samples were successfully cast into the desired shape through this thermal plasticization, flow, and cooling process without the need for solvents to dissolve the polyurethane elastomer. Fig. 7(b) presents the stress-strain curves of the pure GAP-ETPE series (40 %, 45 %, and 50 % hard segment) in the upper left and the PCL-GAP-PCL ETPE series (45 % and 50 % hard segment) in the upper right. The data indicates that the ETPE materials exhibit typical viscoelastic properties [51]. After undergoing permanent deformation, they can resist further stretching, but once failure occurs, they exhibit a contraction phenomenon. We recorded the maximum stress and strain for each ETPE sample. It was observed that for GAP-ETPE, as the proportion of hard segments increased, the maximum stress also increased, while the maximum elongation decreased. From a molecular design point of view, a higher proportion of hard segments implies that more urethane groups are contained in molecular chains available for hydrogen bond formation. As the number of hydrogen bonds increases, the intermolecular connections become tighter, causing the polymers to tend to crystallize. This leads to an increase in macroscopic stress and a decrease in elongation. For example, the 40 % hard segment sample exhibited a maximum stress of 1.28 MPa and a strain of 113 %, whereas the 50 % hard segment sample showed a maximum stress of 3.08 MPa and a strain of 15 %. This series demonstrates that increasing the proportion of hard segments results in higher stress but reduced ductility and increased brittleness of the material [52,53]. In the PCL-GAP-PCL series, a different trend is observed. The 40 % hard segment sample could not be molded successfully. In the variable-temperature IR analysis [Fig. 6(e)], we observed that PCL-GAP-PCL ETPE at 50 % exhibits a lower level of C═O hydrogen bonding compared to GAP-ETPE 50 %. This indicates that, with an equal proportion of amide groups, PCL competes with HMDI for hydrogen bond formation, making it more difficult for HMDI to self-associate into domains. As a result, a higher hard segment content is necessary for successful molding. Consequently, the stress of PCL-GAP-PCL ETPE is lower than that of GAP-ETPE. From AFM images [Fig. S8], it can be seen that GAP-ETPE at 50 % can exhibit distinct hard segment domains, whereas in PCL-GAP-PCL at 50 %, the PCL competes for HMDI amide sites, making the hard segment domains less defined. Despite the presence of hydrogen bonding, it exhibited a flowable

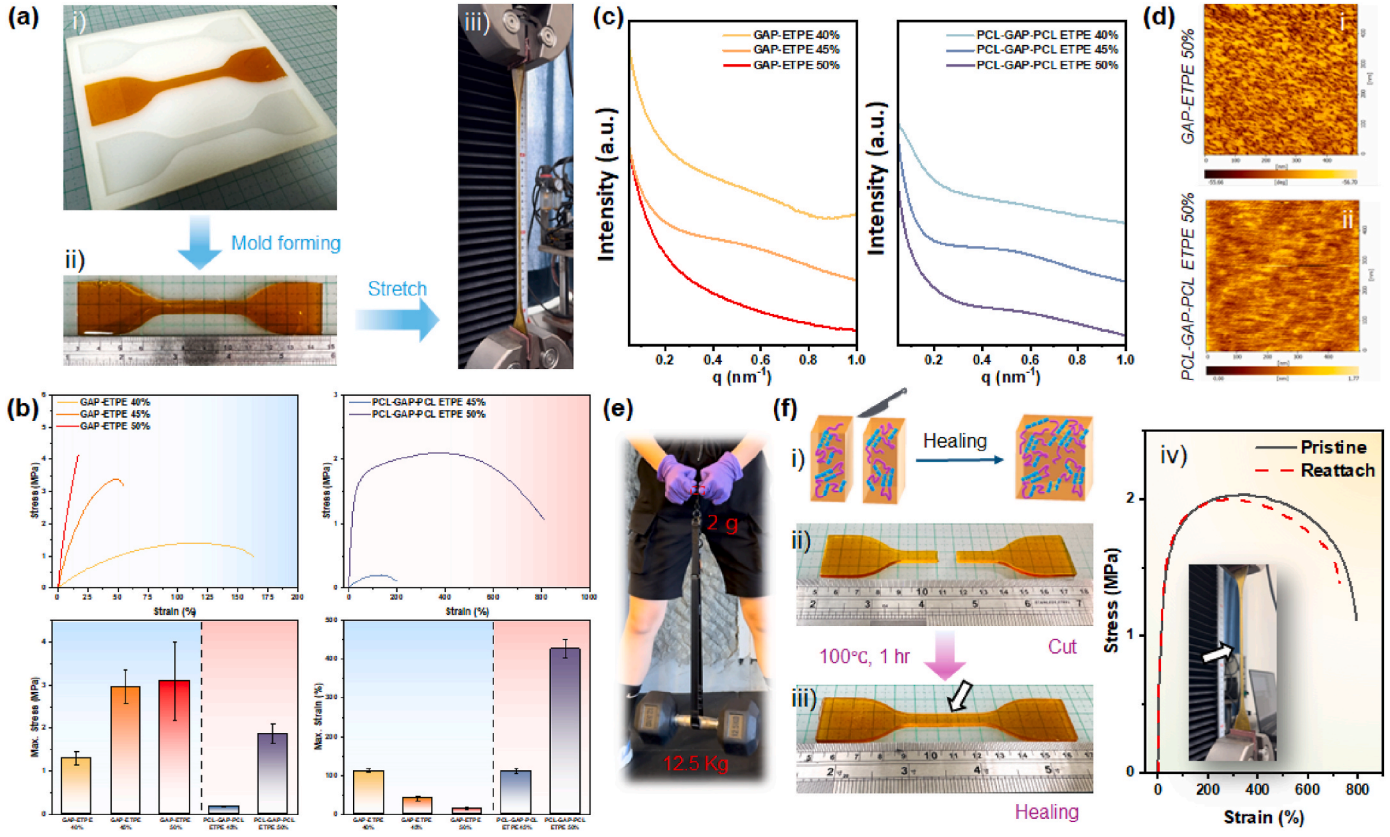

Fig. 7. Structural Analysis of ETPE. (a) Physical properties of thermoplastic energetic elastomers: i. Softening and injection molding of PCL-GAP-PCL ETPE 50 %; ii. Cooling and shaping process; iii. Excellent elongation properties. (b) Stress-strain curve of ETPE. (c) SAXS spectra of ETPE. (d) AFM surface morphology images of GAP-ETPE 40 % and PCL-GAP-PCL ETPE 50 %. (e) Image of PCL-GAP-PCL ETPE 50 % holding a dumbbell. (f) i. Illustration of the healing properties of ETPE; ii. Cutting of PCL-GAP-PCL ETPE 50 %; iii. Healing of PCL-GAP-PCL ETPE 50 %; iv. Original and healed stress-strain curves of PCL-GAP-PCL ETPE 50 %.

deformation state after some time, which was insufficient for it to act as an elastomer. Increasing the hard segment proportion effectively allowed the PCL-GAP-PCL ETPE to be solidified, confirming that a higher hard segment content increases the number of hydrogen bonding sites, facilitating the casting process. Furthermore, it is crucial to note that as the hard segment content increased from 45 % to 50 %, the elastomer did not become brittle. Instead, the maximum stress increased, and the elongation at break improved significantly, reaching up to approximately 8 times the original length (Movie S1). Given that GAP is an ether-based polymer, the incorporation of the ester-based PCL long-chain segments enhances the elongation properties of the material. In the molecular structure of GAP-ETPEs, the soft segments of GAP have only a few sites capable of forming hydrogen bonds, causing the ETPE molecules to rely exclusively on intermolecular hydrogen bond connections, tending to arrange in an orderly orientation. After introducing PCL segments, the soft segment PCL-GAP-PCL triblock prepolymer can also participate in hydrogen bonding, facilitating the formation of both intermolecular and intramolecular hydrogen bonds. When the fraction of hard segments increases from 40 % to 50 %, the crystallinity upsurges, while the elongation contributed by the PCL segments becomes more apparent. This phenomenon corresponds with the crystallization melting point trend shown in Fig. 6(c). In other words, the crystallization characteristic of PCL during the stretching process contributes to improved extensibility [54]. In Fig. 7(c), the SAXS analyses of all ETPE series show a single broad peak with the d-spacing ca. 12.5 nm ($q^* = 0.51\ nm^{-1}$), confirming that our ETPE retains a microphase-separated morphology. This indicates a distinct separation between the soft and hard segments [55]. Similarly, Fig. 7(d) presents AFM surface scans of the samples, where the bright areas represent the hard segments, and the dark regions correspond to the soft segments, clearly showing the presence of microphase separation on the surface [56]. This observation supports the hypothesis that polyester segments provide more hydrogen bonding sites. Notably, the microphase separation in Fig. 7(d-ii) is less pronounced compared to Fig. 7(d–i), suggesting that the interaction between the C═O groups in the soft segments and the N–H groups in the hard segments affects the morphology [57]. As we concluded in our previous discussion on mechanical properties. The molecular chains exhibit a more disordered arrangement than in GAP-ETPE, resulting in expanded intermolecular and intramolecular hydrogen bonds. Since weight-bearing capability is crucial for practical applications of ETPE, we used the normal stress equation ($\sigma = P/A$) to calculate that PCL-GAP-PCL ETPE with 50 % hard segment can support a load of 13.35 kg. This was confirmed experimentally by suspending a 12.5 kg weight from a dumbbell-shaped specimen, with no deformation or rupture observed in Fig. 7(e) and Movie S2. The material load-bearing capacity can also be estimated from the stress-strain curve using the derived equation [49]. ETPE also exhibits excellent healing properties where Fig. 7(f) shows that PCL-GAP-PCL ETPE with 50 % hard segment when kept in a solid state, can heal effectively after the two cut surfaces are brought into contact and heated to 100 °C for 1 h. Post-healing, tensile tests revealed a slight decrease in stress beyond the maximum stress, while the elongation and Young's modulus remained unchanged, demonstrating the material's healing capabilities.

Fig. 8 presents a comparison between the reviewed literature on GAP-ETPE and the results of this study, focusing solely on conditions without the use of plasticizers. The goal is to understand the performance of GAP-ETPE with different hard segment structures compared to previously published GAP-based binder systems, represented by blue spheres [53–57,59]. The PCL-GAP-PCL ETPE with 50 % hard segment prepared in this study exhibits significantly better elongation performance than various GAP-based binder systems utilizing different types of isocyanates. It also demonstrates superior mechanical properties compared to earlier PCL-GAP-PCL systems employing crosslinked networks [31,58]. The PCL-GAP-PCL ETPE from this study is represented by red stars. This improvement is attributed to the flexibility provided by the PCL soft segments. Moreover, the structural similarity between linear GAP and PEO, combined with the presence of azide side chains, contributes to the outstanding elongation behavior when employing PCL-GAP-PCL triblock copolymers as polyols for ETPE synthesis.

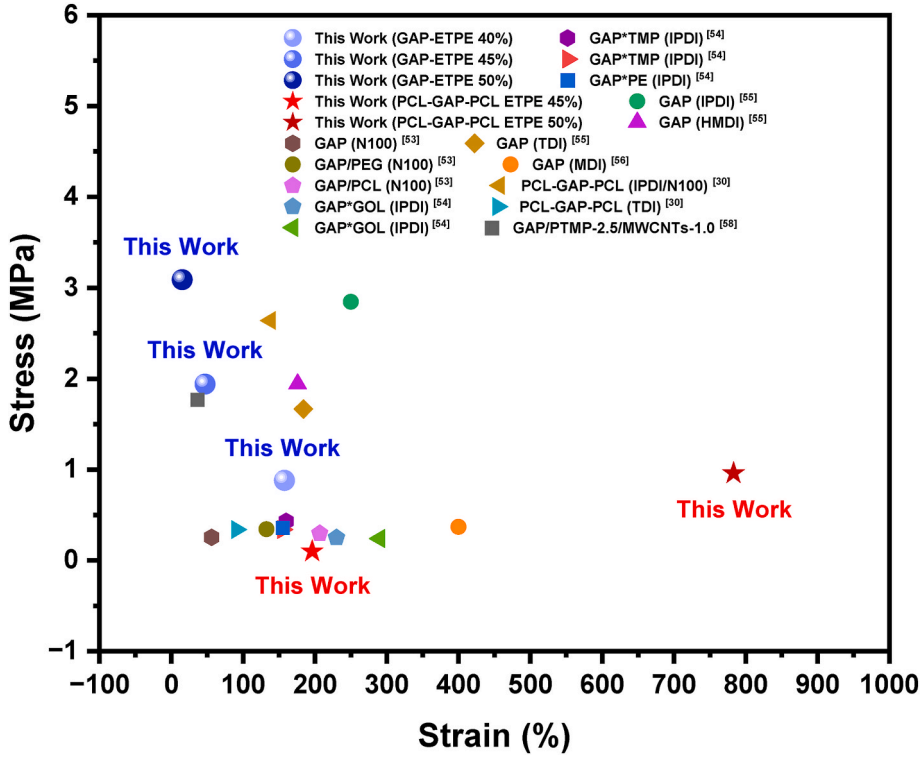

Fig. 8. A comparison of the mechanical properties between this study's results and previously reported GAP-based binder systems in the literature.

4. Conclusion

We successfully synthesized GAP-ETPE and PCL-GAP-PCL ETPE, investigating the process from polymer molecular weight control to ETPE formation. The GAP exhibited an energy capacity of 2386 J/g, while the PCL-GAP-PCL triblock copolymer displayed 1152 J/g. Various ETPEs with different hard segment ratios were prepared. Due to steric constraints from GAP's azido side chains, a higher hard segment ratio was required. Incorporating PCL-GAP-PCL improved tensile properties. GAP-ETPE with 40 % and 45 % hard segment ratios exhibited favorable low-temperature properties and mechanical performance. The 40 % GAP-ETPE showed optimal mechanical and thermal properties, with an energy release of 1390 J/g. PCL-GAP-PCL ETPE also demonstrated promising mechanical properties. Despite a reduced energetic soft segment, the 50 % PCL-GAP-PCL ETPE retained an energy release of 570 J/g. Future incorporation of oxidizers could further enhance thermoplastic solid propellants for green energy applications.

CRediT authorship contribution statement

Ming-Yen Tsai: Writing – original draft, Methodology, Investigation, Formal analysis, Data curation, Conceptualization. **Ming-Chieh Lin:** Methodology, Formal analysis, Data curation, Conceptualization. **Shih-Ya Hong:** Data curation, Conceptualization. **Yi-Chen Wu:** Formal analysis, Data curation. **Mohamed Gamal Mohamed:** Supervision, Methodology, Data curation, Conceptualization. **Shiao-Wei Kuo:** Supervision, Project administration, Funding acquisition.

Declaration of competing interest

The authors declare that they have no known competing financial interests or personal relationships that could have appeared to influence the work reported in this paper.

Acknowledgements

The study was supported by the Armaments Bureau of the Ministry of National Defense Republic of China, National Chung-Shan Institute of Science & Technology, Taiwan, and the National Science and Technology Council, Taiwan (NSTC 113-2223-E-110-001).

Appendix A. Supplementary data

Supplementary data to this article can be found online at https://doi.org/10.1016/j.polymer.2025.128403.

Data availability

The data that has been used is confidential.

References

[1] Y. Wang, L. Hu, S. Pang, J.M. Shreeve, Nitroimino as an energetic group in designing energetic materials for practical use, a tautomerism from nitroamino, J. Mater. Chem. A 11 (2023) 13876–13888, https://doi.org/10.1039/D3TA02235H.

[2] J.Y. Son, S. Aikonen, N. Morgan, A.S. Harmata, J.J. Sabatini, R.C. Sausa, E.F. C. Byrd, D.H. Ess, R.S. Paton, C.R.J. Stephenson, Exploring cuneanes as potential benzene isosteres and energetic materials: scope and mechanistic investigations into regioselective rearrangements from cubanes, J. Am. Chem. Soc. 145 (2023) 16355–16364, https://doi.org/10.1021/jacs.3c03226, oi.org/.

[3] X. Ma, Y. Li, I. Hussain, R. Shen, G. Yang, K. Zhang, Core–shell structured nanoenergetic materials: preparation and fundamental properties, Adv. Mater. 32 (2020) 2001291, https://doi.org/10.1002/adma.202001291.

[4] Y. Qin, F. Yang, S. Jiang, M. Lu, P. Wang, A new breakthrough in electrochemical synthesis of energetic materials: constructing super heat-resistant explosives, Chem. Eng. J. 486 (486) (2024) 149968, https://doi.org/10.1016/j.cej.2024.149968.

[5] W.L. Yuan, L. Zhang, G.H. Tao, S.L. Wang, Y. Wang, Q.H. Zhu, G.H. Zhang, Z. Zhang, Y. Xue, S. Qin, L. He, J.M. Shreeve, Designing high-performance hypergolic propellants based on materials genome, Sci. Adv. 6 (2020) eabb1899, https://doi.org/10.1126/sciadv.abb1899.

[6] R. Xu, M. Yu, Z. Xue, H. Zhang, Q.L. Yan, Enhancing the ignition and combustion performances of solid propellants incorporating Al particles inside oxidizers, ACS Appl. Mater. Interfaces 15 (2023) 56442–56453, https://doi.org/10.1021/acsami.3c11961.

[7] L. Chen, Q. Li, S. Liu, Y. Bei, Y. Ding, J. Liu, W. He, Bio-inspired synthesis of energetic microcapsules core-shell structured with improved thermal stability and reduced sensitivity via in situ polymerization for application potential in propellants, Adv. Mater. Interfac. 8 (2021) 2101248, https://doi.org/10.1002/admi.202101248.

[8] P. Zhang, W. Tan, X. Zhang, J. Chen, J. Yang, J. Deng, Chemical modification of hydroxyl-terminated polybutadiene and its application in composite propellants, J. Ind. Eng. Chem. Res. 60 (2021) 3819–3829, https://doi.org/10.1021/acs.iecr.0c06172.

[9] F. Ghoroghchian, Y. Bayat, F. Abrishami, Preparation of the polyurethane elastomer based on polypropylene glycol- glycidyl azide polymer- polypropylene glycol, J. Polym. Res. 29 (2022) 472, https://doi.org/10.1007/s10965-022-03292-z.

[10] J.C.Q. Amado, P.G. Ross, L.M.S. Murakami, J.C.N. Durta, Properties of hydroxyl-terminal polybutadiene (HTPB) and its use as a liner and binder for composite propellants: a review of recent advances, Propellants, Explos. Pyrotech. 47 (2022) e202100283, https://doi.org/10.1002/prep.202100283.

[11] K. Nachtrieb, C. Nie, P.J. Chirik, M.M. Beromi, Synthesis, thermochemistry, and cure behavior of Oligocyclobutane-Containing prepolymers relevant to propellant applications, ACS Appl. Polym. Mater. 6 (2024) 5171–5182, https://doi.org/10.1021/acsapm.4c00316.

[12] Y. Wen, H. Mo, B. Tan, X. Lu, B. Wang, N. Liu, Progress in synthesis and properties of oxetane–based energetic polymers, Eur. Polym. J. 194 (2023) 112161, https://doi.org/10.1016/j.eurpolymj.2023.112161.

[13] Y. Hu, G. Tang, Y.Y. Luo, S. Chi, X. Li, Glycidyl azide polymer-based polyurethane vitrimers with disulfide chain extenders, Polym. Chem. 12 (2021) 4072–4082, https://doi.org/10.1039/D1PY00441G.

[14] L. Zhang, X. Su, S. Wang, X. Li, M. Zou, In situ preparation of Al@3-Perfluorohexyl-1, 2-epoxypropane@glycidyl azide polymer (Al@PFHP@GAP) high-energy material, Chem. Eng. J. 450 (2022) 137118, https://doi.org/10.1016/j.cej.2022.137118.

[15] J.J. Sabatini, E.C. Johnson, A short review of nitric esters and their role in energetic materials, ACS Omega 6 (2021) 11813–11821, https://doi.org/10.1021/acsomega.1c01115.

[16] Y. Huang, J. Gao, Y. Chen, Y. Zang, J. Sun, C. Zhang, Azide polyether with a highly flexible main chain as energetic materials, ACS Appl. Polym. Mater. 5 (2023) 3096–3103, https://doi.org/10.1021/acsapm.3c00241.

[17] M. Born, K. Karaghiosoff, T.M. Klapotke, A GAP replacement: improved synthesis of 3-Azidooxetane and its homopolymer based on sulfonic acid esters of Oxetan-3-ol, J. Org. Chem. 86 (2021) 12607–12614, https://doi.org/10.1021/acs.joc.1c01060.

[18] Y.M. Mohan, K.M. Raju, Synthesis and characterization of HTPB-GAP cross-linked co-polymers, Des. Monomers Polym. 8 (2005) 159–175, https://doi.org/10.1163/1568555053603215.

[19] J.S. You, S.C. Kang, S.K. Kweon, H.L. Kim, Y.H. Ahn, S.Y. Noh, Thermal decomposition kinetics of GAP ETPE/RDX-based solid propellant, Thermochim. Acta 737 (2012) 51–56, https://doi.org/10.1016/j.tca.2012.02.032.

[20] G. Zhan, J. Wang, X. Liu, M. Li, C. Chen, N. Wang, X. Hou, Correlation between the micro-structure and macroscopic mechanical properties of GAP-Based propellant during aging, Polym. Degrad. Stabil. 214 (2023) 110411, https://doi.org/10.1016/j.polymdegradstab.2023.110411.

[21] G. Tang, D.L. Wang, Y.J. Luo, X.Y. Li, Novel azide-rich fluorinated energetic polyurethane with excellent mechanical properties by a one-pot facile strategy, Eur. Polym. J. 177 (2022) 111428, https://doi.org/10.1016/j.eurpolymj.2022.111428.

[22] T. Jarosz, A. Stolarczyk, A. Wawrzkiewicz-Jalowiecka, K. Pawlus, K. Miszczyszyn, Glycidyl azide polymer and its derivatives-versatile binders for explosives and pyrotechnics: tutorial review of recent progress, Molecules 24 (2019) 4475, https://doi.org/10.3390/molecules24244475.

[23] M.L. Guo, Z.L. Ma, L.M. He, W. He, Y.W. Wang, Effect of varied proportion of GAP-ETPE/NC as binder on thermal decomposition behaviors, stability and mechanical properties of nitramine propellants, J. Therm. Anal. Calorim. 130 (2017) 909, https://doi.org/10.1007/s10973-017-6351-z.

[24] P. Zhao, L. Chen, Q. Zhang, Y. Ling, Q. Lin, H. Huang, Y. Yang, A green oxidizer based on 1,2,3-triazole with a high oxygen balance of +23.3%: a promising replacement of ammonium perchlorate in solid propellants, J. Mater. Chem. A 12 (2024) 13682–13688, https://doi.org/10.1039/D4TA01653J.

[25] T.X. Liang, Y.K. Zhang, Z.L. Ma, M.L. Guo, Z.L. Xiao, J.X. Zhang, M.Y. Dong, J. C. Fan, Z.H. Guo, C.T. Liu, Energy characteristics and mechanical properties of cyclotrimethylenetrinitramine (RDX)-Based insensitive high-energy propellant, J. Mater. Res. Technol. 9 (2020) 15313, https://doi.org/10.1016/j.jmrt.2020.09.132.

[26] X.Y. Miao, R. Han, J. Tian, Y.C. Ma, A.J. Müller, Z.B. Li, Achieving high fill factor in organic photovoltaic cells by tuning molecular electrostatic potential fluctuation, Angew. Chem. Int. Ed. 63 (2024) e202417627, https://doi.org/10.1002/anie.202401066.

[27] T.C. Chou, S.W. Kuo, Controllable wet-brush blending of linear diblock copolymers with Phenolic/DDSQ hybrids toward mesoporous structure phase diagram, Macromolecules 57 (2024) 5958–5970, https://doi.org/10.1021/acs.macromol.4c00665.

[28] Y.C. Huang, W.C. Chen, S.W. Kuo, Mesoporous Phenolic/POSS hybrids induced by microphase separation arising from competitive hydrogen bonding interactions, Macromolecules 55 (2022) 8918–8930, https://doi.org/10.1021/acs.macromol.2c01585.
[29] J.G. Li, Y.F. Ho, M.M.M. Ahmed, H.C. Liang, S.W. Kuo, Mesoporous carbons templated by PEO-PCL block copolymers as electrode materials for supercapacitors, Chem. Eur J. 25 (2019) 10456–10463, https://doi.org/10.1002/chem.201901724.
[30] B.S. Min, Characterization of the plasticized GAP/PEG and GAP/PCL block copolyurethane binder matrices and its propellants, Propellants, Explos. Pyrotech. 33 (2008) 131, https://doi.org/10.1002/prep.200700241.
[31] J.S. You, S.T. Noh, Thermal and mechanical properties of poly(glycidyl azide)/polycaprolactone copolyol-based energetic thermoplastic polyurethanes, Macromol. Res. 18 (2010) 1081, https://doi.org/10.1007/s13233-010-1104-x.
[32] C. Tantisuwanno, T. Jain, Y.M. Tseng, A. Joy, Pendant amines in the hard or soft segments of PCL-polyurethanes have contrasting effects on the mechanical and surface properties, Macromolecules 57 (2024) 4448–4459, https://doi.org/10.1021/acs.macromol.3c02292.
[33] W. Hu, C. Qi, X. Guo, A.M. Pang, N. Zhou, J. Lu, G. Tang, L. Gan, J. Huang, Alkynyl-functionalization of carbon nanotubes to promote anchoring potential in glycidyl azide polymer-based binders via huisgen reaction for solid propellant application, J. Polym. Res. 28 (2021) 126, https://doi.org/10.1007/s10965-021-02468-3.
[34] Y.M. Mohan, K.M. Raju, B. Sreedhar, Synthesis and characterization of glycidyl azide polymer with enhanced azide content, Int. J. Polym. Mater. 72 (2015) 1835–1847, https://doi.org/10.1080/009140390970486.
[35] G. Shukla, R.C. Ferrier, The versatile, functional polyether, polyepichlorohydrin: history, synthesis, and applications, J. Polym. Sci. 59 (2021) 2704–2718, https://doi.org/10.1002/pol.20210514.
[36] T. Biedron, P. Kubisa, S. Penczek, Polyepichlorohydrin diols free of cyclics: synthesis and characterization, J. Polym. Sci., Polym. Chem. Ed. 29 (1991) 619, https://doi.org/10.1002/pola.1991.080290502.
[37] S.K. Reshmi, K.P. Vijayalakshmi, D. Thomas, E. Arunan, C.P. Reghunadhan Nair, Glycidyl azide polymer crosslinked through triazoles by click chemistry: curing, mechanical and thermal properties, Propellants, Explos. Pyrotech. 38 (2013) 525–532, https://doi.org/10.1002/prep.201200036.
[38] S. Pisharath, H.G. Ang, Synthesis and thermal decomposition of GAP–Poly(BAMO) copolymer, Polym. Degrad. Stabil. 92 (2007) 1365, https://doi.org/10.1016/j.polymdegradstab.2007.03.016.
[39] Y. Haas, Y. Beneliahu, S. Welner, Infrared laser-induced decomposition of GAP, Combust. Flame 96 (1994) 212–220, https://doi.org/10.1016/0010-2180(94)90010-8.
[40] Y. Bakkour, V. Darcos, S.M. Li, J. Coudane, Diffusion ordered spectroscopy (DOSY) as a powerful tool for amphiphilic block copolymer characterization and for critical micelle concentration (CMC) determination, Polym. Chem. 3 (2012) 2006–2010, https://doi.org/10.1039/C2PY20054F.
[41] W.T. Du, S.Y. Chen, S.W. Kuo, Mesoporous phenolic/carbon materials templated by CO_2-based PEO-b-PCHC diblock copolymers through mediated competitive intermolecular hydrogen bonding interactions for CO_2 capture, J. CO2 Util. 80 (2024) 102702, https://doi.org/10.1016/j.jcou.2024.102702.
[42] S.W. Kuo, C.F. Huang, F.C. Chang, Study of hydrogen-bonding strength in poly (ε-caprolactone) blends by DSC and FTIR, J. Polym. Sci., Part B: Polym. Phys. 39 (2001) 1348–1359, https://doi.org/10.1002/polb.1107.
[43] S.W. Kuo, C.L. Lin, F.C. Chang, Phase behavior and hydrogen bonding in ternary polymer blends of phenolic resin/poly(ethylene oxide)/Poly(ε-caprolactone), Macromolecules 35 (2002) 278–285, https://doi.org/10.1021/ma011255f.
[44] J.G. Li, Y.D. Lin, S.W. Kuo, From microphase separation to self-organized mesoporous phenolic resin through competitive hydrogen bonding with double-crystalline diblock copolymers of poly(ethylene oxide-b-ε-caprolactone), Macromolecules 44 (2011) 9295–9309, https://doi.org/10.1021/ma2010734.
[45] S.W. Kuo, Hydrogen Bonding in Polymeric Materials, Wiley-VCH, Weinheim, 2018.
[46] C. Tantisuwanno, T. Jain, Y.M. Tseng, A. Joy, Synthesis and characterization of segmented polyurethanes containing trisaminocyclopropenium carbocations, Macromolecules 67 (2024) 4448–4459, https://doi.org/10.1021/acsmacrolett.8b00395.
[47] I. Noda, Two-dimensional infrared spectroscopy, J. Am. Chem. Soc. 111 (1989) 8116–8118, https://doi.org/10.1021/ja00203a008.
[48] J.H. Xu, Y.Y. Chen, Y.N. Zhang, T. Liu, J. Fu, A fast room-temperature self-healing glassy polyurethane, Angew. Chem., Int. Ed. 60 (2024) 7947–7955, https://doi.org/10.1002/anie.202017303.
[49] S.W. Kuo, H.C. Lin, W.J. Huang, C.F. Huang, F.C. Chang, Hydrogen bonding interactions and miscibility between phenolic resin and octa(acetoxystyryl) polyhedral oligomeric silsesquioxane (AS-POSS) nanocomposites, J. Polym. Sci., Part B: Polym. Phys. 44 (2006) 673–686, https://doi.org/10.1002/polb.20731.
[50] T.L. Ma, W.T. Du, S.W. Kuo, Design and mediated hydrogen bonding strength of Poly(styrene-alt- N–(ethyl–4–hydroxyphenyl)maleimide) copolymer to enhance miscibility with hydrogen bonded acceptor homopolymers, Polymer 311 (2024) 127574, https://doi.org/10.1016/j.polymer.2024.127574.
[51] C.F. Wu, Y.Y. Lu, M. Jiang, S.Q. Hu, H.T. Yang, X.L. Fu, H.Y. Li, Study on mechanical properties and failure mechanisms of highly filled hydroxy-terminated polybutadiene propellant under different tensile loading conditions, Polymers 15 (2023) 3869, https://doi.org/10.3390/polym15193869.
[52] T.J. Touchet, E.M. Cosgriff-Hernandez, in: S.L. Cooper, J. Guan (Eds.), Advances in Polyurethane Biomaterials, Woodhead Publishing, 2016.
[53] T.T. Guan, X.H. Wang, Y.L. Zhu, L. Qian, Z.Y. Lu, Y.F. Men, J. Li, Y.T. Wang, J. Q. Sun, Mechanically robust skin-like poly(urethane-urea) elastomers cross-linked with hydrogen-bond arrays and their application as high-performance ultrastretchable conductors, Macromolecules 55 (2022) 5816–5825, https://doi.org/10.1021/acs.macromol.2c00492.
[54] B.P. Grady, S.L. Cooper, C.G. Robertson, The Science and Technology of Rubber, Academic Press, Boston, 2013, p. 591.
[55] B.X. Cheng, W.C. Gao, X.M. Ren, X.Y. Ouyang, Y. Zhao, H. Zhao, W. Wu, C. X. Huang, Y. Liu, X.Y. Liu, H.N. Li, R.K.Y. Li, A review of microphase separation of polyurethane: characterization and applications, Polym. Test. 107 (2022) 107489, https://doi.org/10.1016/j.polymertesting.2022.107489.
[56] J.J. Zhang, Applied Petroleum Geomechanics, Gulf Professional Publishing, 2019, pp. 1–27.
[57] S. Zhang, W. Hu, L. Gan, G. Tang, X. Guo, A.M. Pang, J. Huang, Inserting urethane into 1,2,3-Triazole click-cured solid propellant binder to form microphase separation and enhance mechanical and combustible performances, J. Appl. Polym. Sci. 140 (2023) 41, https://doi.org/10.1002/app.54522.
[58] M. Chizari, Y. Bayat, Designing a highly energetic PCL-GAP-PCL-based PU elastomer; investigation of the effect of plasticizers on its properties, Cent. Eur. J. Energ. Mater. 16 (2019) 33–48, https://doi.org/10.22211/cejem/104386.
[59] S. Wang, C. Liu, X. Guo, G. Tang, L. Gan, C. Qi, J. Huang, Effects of crosslinking degree and carbon nanotubes as filler on composites based on glycidyl azide polymer and propargyl-terminated polyether for potential solid propellant application, J. Appl. Polym. Sci. 134 (2017) 39, https://doi.org/10.1002/app.45359.